JACS
JOURNAL OF THE AMERICAN CHEMICAL SOCIETY
Article
pubs.acs.org/JACS

# Biohybrid Photosynthetic Antenna Complexes for Enhanced Light-Harvesting

Joseph W. Springer,[†] Pamela S. Parkes-Loach,[‡] Kanumuri Ramesh Reddy,[§] Michael Krayer,[§] Jieying Jiao,[⊥] Gregory M. Lee,[‡] Dariusz M. Niedzwiedzki,[†,∥] Michelle A. Harris,[†] Christine Kirmaier,[†] David F. Bocian,*[,⊥] Jonathan S. Lindsey,*[,§] Dewey Holten,*[,†] and Paul A. Loach*[,‡]

[†]Department of Chemistry and [∥]Photosynthetic Antenna Research Center, Washington University, St. Louis, Missouri 63130-4889, United States

[‡]Department of Molecular Biosciences, Northwestern University, Evanston, Illinois 60208-3500, United States

[§]Department of Chemistry, North Carolina State University, Raleigh, North Carolina 27695-8204, United States

[⊥]Department of Chemistry, University of California, Riverside, California 92521-0403, United States

Supporting Information

**ABSTRACT:** Biohybrid antenna systems have been constructed that contain synthetic chromophores attached to 31mer analogues of the bacterial photosynthetic core light-harvesting (LH1) $\beta$-polypeptide. The peptides are engineered with a Cys site for bioconjugation with maleimide-terminated chromophores, which include synthetic bacteriochlorins (**BC1**, **BC2**) with strong near-infrared absorption and commercial dyes Oregon green (**OGR**) and rhodamine red (**RR**) with strong absorption in the blue-green to yellow-orange regions. The peptides place the Cys 14 (or 6) residues before a native His site that binds bacteriochlorophyll *a* (BChl-*a*) and, like the native LH proteins, have high helical content as probed by single-reflection IR spectroscopy. The His residue associates with BChl-*a* as in the native LH1 $\beta$-polypeptide to form dimeric $\beta\beta$-subunit complexes $[31\text{mer}(-14\text{Cys})\text{X/BChl}]_2$, where X is one of the synthetic chromophores. The native-like BChl-*a* dimer has $Q_y$ absorption at 820 nm and serves as the acceptor for energy from light absorbed by the appended synthetic chromophore. The energy-transfer characteristics of biohybrid complexes have been characterized by steady-state and time-resolved fluorescence and absorption measurements. The quantum yields of energy transfer from a synthetic chromophore located 14 residues from the BChl-coordinating His site are as follows: **OGR** (0.30) < **RR** (0.60) < **BC2** (0.90). Oligomeric assemblies of the subunit complexes $[31\text{mer}(-14\text{Cys})\text{X/BChl}]_n$ are accompanied by a bathochromic shift of the $Q_y$ absorption of the BChl-*a* oligomer as far as the 850-nm position found in cyclic native photosynthetic LH2 complexes. Room-temperature stabilized oligomeric biohybrids have energy-transfer quantum yields comparable to those of the dimeric subunit complexes as follows: **OGR** (0.20) < **RR** (0.80) < **BC1** (0.90). Thus, the new biohybrid antennas retain the energy-transfer and self-assembly characteristics of the native antenna complexes, offer enhanced coverage of the solar spectrum, and illustrate a versatile paradigm for the construction of artificial LH systems.

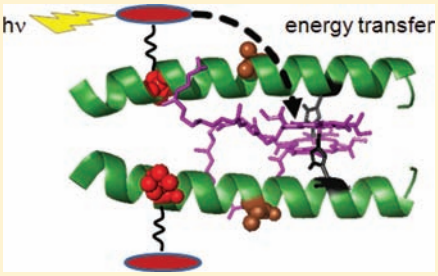


## 1. INTRODUCTION

The quest for renewable energy has prompted substantial interest in evaluating the attributes and limitations of natural photosynthetic processes.[1] Both plant and bacterial photosynthetic systems employ light-harvesting antenna systems that collect light and funnel energy to the reaction centers. The antennas are generally multi-subunit complexes that simultaneously (i) hold the light-absorbing cofactors—(bacterio)chlorophylls and accessory chromophores—at fixed relative distances and orientations, (ii) tune the absorption wavelengths of these chromophores, and (iii) achieve directional energy funneling.[2,3] These combined features give rise to nearly quantitative delivery of the energy quanta to the photochemical reaction centers. Despite this high quantum yield, the overall photoconversion efficiency is limited at the outset because a given photosynthetic antenna system utilizes only a fraction (typically less than half) of the photon-rich visible and near-infrared (NIR) regions of the solar spectrum.[1] Thus, in the construction of highly efficient artificial solar-conversion systems, it is important to maximize solar coverage while maintaining near-quantitative delivery to the target sites.

The mainstream efforts over the past few decades to build fully synthetic light-harvesting systems have required constructing both the chromophores and scaffolding *de novo*.[4,5] The challenges associated with such syntheses have chiefly restricted focus to architectures containing chromophores that are relatively few in number (e.g., <10) and have readily accessible synthetic chemistry (e.g., porphyrins, which lack red and NIR absorption).[6] A complementary approach entails development of biohybrid light-harvesting systems. The biohybrid approach builds upon the burgeoning structural knowledge of the natural

**Received:** August 10, 2011
**Published:** February 29, 2012

   dx.doi.org/10.1021/ja207390y | *J. Am. Chem. Soc.* 2012, 134, 4589−4599

light-harvesting (bacterio)chlorophyll–protein complexes,[7−10] the ability to reconstitute bacterial antenna systems from the component parts *in vitro*,[11−14] and the recent availability of red- and NIR-absorbing, stable synthetic (bacterio)chlorins.[15−19] The bacteriochlorins are distinguished by wavelength tunability of a sharp and intense absorption band in the NIR region, a reasonable degree of synthetic tailorability (for solubility, bioconjugation, etc.), robustness on routine handling, and spectral features that are quite insensitive to medium and environmental polarity.[15] Few if any other classes of pigments afford this combination of features,[20] and few bioconjugatable bacteriochlorins have previously been prepared.[6,21,22]

A foundation for developing biohybrid antenna complexes relies on modifications of the $\alpha\beta$-subunit (Figure 1A) common

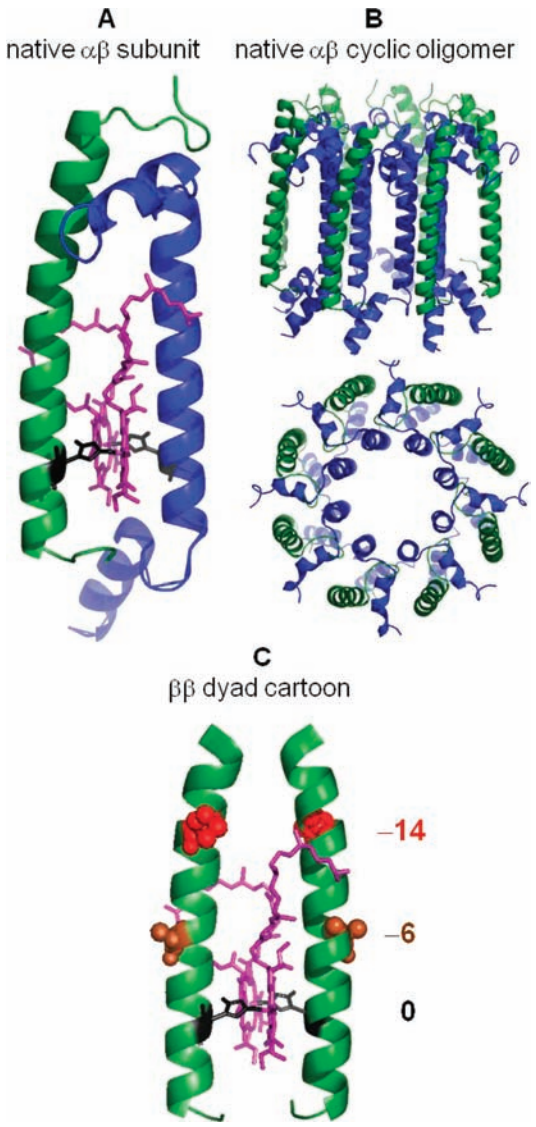


**Figure 1.** (A) $\alpha\beta$-Subunit of the LH2 (B800–850) complex of *Rs. molischianum*.[9] (B) Side and top views of the full LH2 complex showing polypeptides without BChl-*a* for clarity. (C) Cartoon of the 31mer $\beta\beta$-complex showing two possible sites (−14, −6) for chromophore attachment and the BChl-*a* dimer B820 (purple). The BChl-coordinated His (black) is defined as position 0.

to cyclic oligomeric light-harvesting complexes LH1 and LH2 (Figure 1B) of photosynthetic bacteria.[7−9] The subunit consists of two polypeptides ($\alpha$ and $\beta$), both of which are typically 40–50 amino acids in length[2,12] and contribute a histidine residue (Figure 1A, black) as an apical ligand to the central Mg of one of two bacteriochlorophyll *a* (BChl-*a*) molecules in the subunit complex (Figure 1A, purple). Electronic interactions between the two BChl-*a* molecules shift the intense $Q_y$ absorption band from ∼780 nm for monomeric BChl-*a* to ∼820 nm for the dyad. The $\alpha\beta$-subunit readily self-assembles from the native components ($\alpha$ and $\beta$ polypeptides and BChl-*a*) *in vitro*.[11−14]

In this paper, we describe the design, assembly, and energy-transfer characteristics of biohybrid antenna complexes. For the construction of these complexes, polypeptide analogues containing the last 31 amino acids of the $\beta$ polypeptide of *Rb. sphaeroides* LH1[11,23,24] have been utilized. These polypeptides lack 17 residues from the N-terminus of the native peptide and have the sequence ELHSVY**M**$^{-14}$SGLWLFS**A**$^{-6}$VAIVA**H**$^{0}$LAVYIWRPWF. (Three key sites are shown bold and underlined with positions superscripted.) Prior work has shown that the 31mer readily associates with BChl-*a* to form a homodimeric $\beta\beta$-subunit complex (illustrated in Figure 1C) in which the BChl-*a* dimer (denoted B820) has a $Q_y$ absorption band near 820 nm.[11,23,24] Oligomeric forms can be produced in which the BChl-*a* $Q_y$ band is bathochromically shifted to up to 850 nm (and thus denoted B850). In our studies, two peptide analogues were prepared in which either −6Ala (Figure 1C, brown) or −14Met (Figure 1C, red) is replaced by Cys to allow designer–chromophore attachment at that site. The modified 31mers (without attached chromophore) are denoted 31mer(−6Cys) and 31mer(−14Cys). The chromophores chosen for covalent attachment to the peptides include two synthetic bacteriochlorins (**BC1**, **BC2**) and two commercial dyes [Oregon green (**OGR**) and rhodamine red (**RR**)] (Figure 2). Each

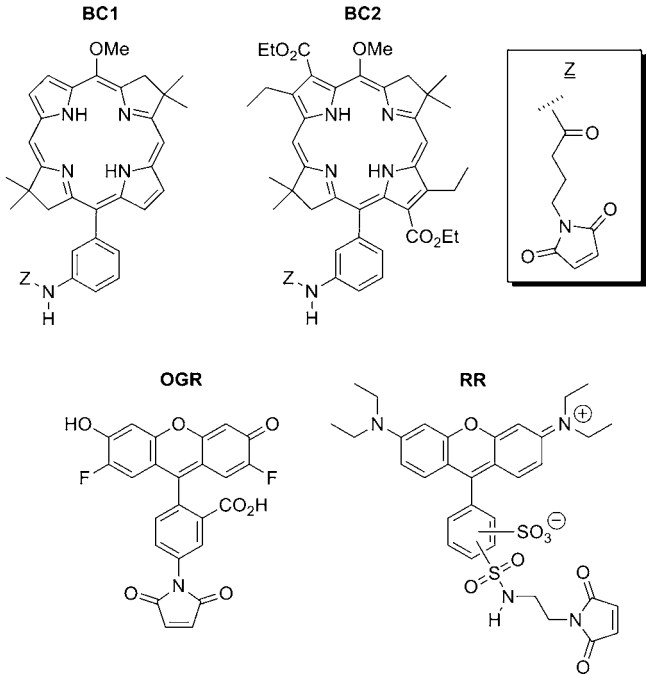


**Figure 2.** Bioconjugatable bacteriochlorins (**BC1**, **BC2**) and commercial dyes (**OGR**, **RR**).

chromophore bears a maleimide-terminated linker for bioconjugation with the Cys site of 31mer(−6Cys) and 31mer(−14Cys). These four chromophores have spectral properties that are complementary to each other and to the BChl-*a* energy-acceptor complex in the biohybrid antennas.


dx.doi.org/10.1021/ja207390y | *J. Am. Chem. Soc.* 2012, 134, 4589–4599

The biohybrid complexes thus afford a modular design and synthesis, can draw on a palette of diverse bioconjugatable dyes, exploit natural self-assembling peptides, and afford the possibility to tailor the desired absorption spectral features in the creation of antenna systems with enhanced light-harvesting capacity.

## 2. EXPERIMENTAL PROCEDURES

Two synthetic polypeptides (Bio-Synthesis, Lewisville, TX) were used in these studies. Each contained 31 amino acids with a sequence identical to that of the last 31 amino acids in the $\beta$ polypeptide of LH1 of *Rb. sphaeroides* except for the substitution of a Cys in place of either Met-14 or Ala-6. Purity was >90% according to HPLC data, and the mass spectrometry results were consistent with the expected product: $m/z$ = 3633 observed versus 3634 calculated for the 31mer(−14Cys), and $m/z$ = 3694 observed versus 3696 calculated for the 31mer(−6Cys). BChl-*a* with a geranyl-geraniol esterifying alcohol was isolated from membranes of the G9 carotenoidless mutant of *Rhodospirillum rubrum*.[24] *n*-Octyl $\beta$-D-glucopyranoside (referred to as octyl glucoside) from Sigma and the dyes Oregon green 488 maleimide (**OGR**) and rhodamine red maleimide (**RR**) from Invitrogen: Molecular Probes were used as received. The synthesis of the bacteriochlorins **BC1** and **BC2** will be described elsewhere. The synthetic chromophores were tethered to the peptides in *N,N*-dimethylformamide via standard procedures to afford 1:1 complexes of dye:peptide on the basis of extinction coefficients for each of **BC2**, **OGR**, and **RR** (see Supporting Information). For **BC1**, limited solubility in the HPLC solvents precluded rigorous removal of unreacted 31mer(−14Cys) from 31mer(−14Cys)BC1. If any **BC1**-free peptide were incorporated into the biohybrid complexes, the amount and effect are small on the basis of the agreement of the energy-transfer efficiency determined from fluorescence excitation spectra versus two other measurements, as described below.

The conditions for forming B820- and B850-type complexes have been previously described.[11,23,24] In general, 0.05−0.20 mg of each polypeptide was dissolved in 5−10 $\mu$L of hexafluoroacetone trihydrate. To this solution was added 0.50 mL of 4.5% (w/v) octyl glucoside in 50 mM potassium phosphate buffer (pH 7.5), followed by 2.0 mL of 100 mM potassium phosphate buffer (pH 7.5) to bring the octyl glucoside concentration to 0.90%. Increasing amounts of BChl-*a* were then added to the sample by injecting 5−20 $\mu$L of a degassed acetone solution to approach the same BChl-*a* concentration as that of the polypeptide. In general, this resulted in a combined absorbance ($A_{780nm} + A_{820nm}$) between 0.1 and 0.2. The sample was then diluted to 0.75% octyl glucoside and again to 0.66% octyl glucoside to optimize subunit formation. After each dilution, an absorption spectrum was recorded. In some cases, complete formation of the B820 complex required cooling the sample to about 6 °C for 1 h. For formation of B850-type complexes, the sample was kept overnight at 4−8 °C, after which a final absorption spectrum was taken. For evaluation of the B850-type complex stability, the samples (after chilling overnight) were brought to room temperature and the absorption spectra recorded over time to follow the conversion to B820 and/or BChl-*a*. For study of the B850-type complexes at room temperature, the samples that were chilled overnight were diluted with an equal volume of cold 100 mM potassium phosphate buffer (pH 7.5) to bring the octyl glucoside concentration to 0.33% and then warmed to room temperature. Prior to reconstitution, protein concentrations were determined by dissolving the protein in 20 $\mu$L of hexafluoroacetone trihydrate followed by 1.00 mL of 0.1% TFA in 2:1 (v/v) acetonitrile/2-propanol,[24] recording the UV absorption spectrum, and calculating the concentration assuming an extinction coefficient at 287 nm of 3400 $M^{-1}$ $cm^{-1}$ per Trp residue.[25] Where necessary, a correction was made for the absorbance of the attached chromophores. Aliquots were dried under argon and vacuum. The B820- and B850-type complexes were prepared at Northwestern University and shipped overnight on ice (in their B850 state) to Washington University, where they were stored at 4−8 °C.

Procedures for single-reflection infrared spectroscopy, ellipsometry, and steady-state and time-resolved optical spectroscopy are described in the Supporting Information.

## 3. RESULTS AND DISCUSSION

**3.1. Synopsis.** In the following, the assembly of the new biohybrid architectures from the component parts is described first (section 3.2). The energy-transfer properties of the dimeric $\beta\beta$-subunit complexes are then given (section 3.3), followed by a description of the results of studies of energy flow in oligomeric assemblies based on the same components (section 3.4). A general analysis of the results for the various biohybrid complexes is then given and related to the Förster theory for energy transfer (section 3.5). Finally, conclusions and an outlook for future directions are presented (section 4).

**3.2. Assembly of Biohybrid Light-Harvesting Complexes.** *3.2.1. Properties of the Components.* The synthetic analogues of the native antenna peptides, both with and without attached chromophores, were examined to ensure that they retained helical structures (like the native $\beta$ polypeptide[26−28]). Figure 3 shows single-reflection FTIR spectra of 31mer(−14Cys),

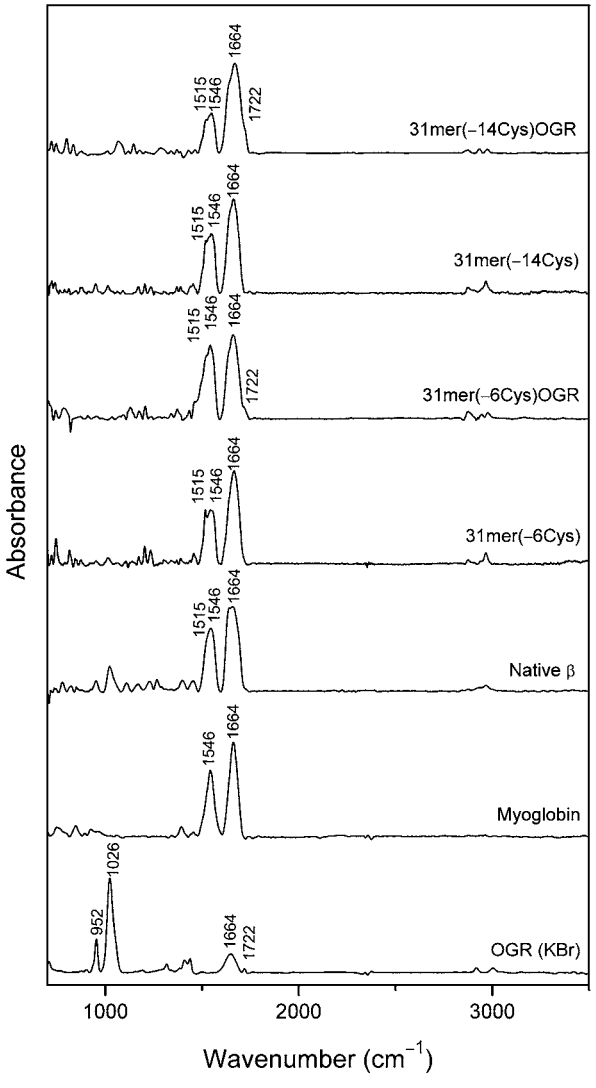


**Figure 3.** Single-reflection FTIR spectra of antenna peptides and myoglobin in films on gold (15 h deposition time) and **OGR** in KBr pellet.


dx.doi.org/10.1021/ja207390y | J. Am. Chem. Soc. 2012, 134, 4589−4599

31mer(−6Cys), both peptides with attached **OGR**, the native $\beta$ peptide, and myoglobin films on gold, as well as **OGR** in a KBr pellet. Myoglobin serves as a model for a prototypical $\alpha$-helical system and exhibits two strong bands at 1664 and 1546 $cm^{-1}$, assignable to the amide I and amide II vibrations. The various peptides, with and without the conjugated **OGR**, exhibit similar spectra, consistent with an $\alpha$-helical structure. Comparisons among the spectra lead to several conclusions: (i) Deposition on the metal substrate does not disrupt the structure of the peptide. (ii) The comparable spectra for 31mer(−14Cys) versus 31mer(−14Cys)OGR and 31mer(−6Cys) versus 31mer(−6Cys)OGR indicate that attachment of **OGR** does not significantly perturb the $\alpha$-helical content of the peptide. (iii) The similarity in the spectra of the 31mer peptides and full-length native $\beta$ indicates that the 31mers retain significant $\alpha$-helical content despite removal of 17-residues from the N-terminus of the native sequence. Finally, no bands are apparent in the IR spectra of peptides 31mer(−14Cys)OGR and 31mer(−6Cys)OGR that might be attributed to **OGR**. This observation is not surprising, given that there is a single dye molecule attached to the protein and that all the amino acid residues collectively contribute to the IR spectrum. The high $\alpha$-helical content of the polypeptides and their conjugated derivatives in films is consistent with NMR studies of the native $\beta$-polypeptide in organic solvents[26,28] and in aqueous detergent solutions[27] as well as the crystal structures for LH2 of *Rs. molischianum*[9] (Figure 1), *Rps. acidophila*,[7] and the RC-LH1 complex[8] of *Rps. palustris*. Thus, the backbone structures of the 31mer polypeptides and their chromophore-tethered forms are essentially known in their B820- and oligomeric-type complexes.

One long-term objective of the studies of the biohybrid systems is to form extended assemblies on solid substrates. Consequently, other properties of the peptides on the surface were investigated. These properties included the thickness of the films formed as a function of deposition time and the helicity of the peptides as a function of film thickness. Elipsometric measurements as a function of deposition time (10 min to 15 h) revealed that the average film thickness increases as a function of deposition time and maximizes at ∼5−7 nm (Figure S-2). This thickness corresponds to an extremely thin film of ∼10 peptides if the peptides lie flat on the surface, or a single monolayer if the peptides assemble vertically. Regardless of film thickness, the $\alpha$-helicity of the peptides does not change, as judged by the frequencies of the amide I and II vibrations.

The chromophores for bioconjugation to the synthetic peptides have complementary optical properties. Figure 4 shows the longest wavelength absorption band and the fluorescence profile for chromophores **BC1**, **BC2**, **OGR**, and **RR** (normalized for clarity). The bacteriochlorins have an intense ($\varepsilon \approx 120\,000\ M^{-1}\ cm^{-1}$)[15,19] NIR $Q_y$ band plus weaker $Q_x$ bands (500−560 nm) and strong near-UV Soret bands (not shown). **OGR** ($\varepsilon \approx 77\,000\ M^{-1}\ cm^{-1}$) and **RR** ($\varepsilon \approx 126\,000\ M^{-1}\ cm^{-1}$) absorb and fluoresce strongly in the blue-green and yellow-orange spectral regions, respectively (450−650 nm) (see Supporting Information).

*3.2.2. Formation of B820- and Oligomeric-Type Complexes.* Both 31mer(−14Cys) and 31mer(−6Cys) associate with BChl-*a* to form $\beta\beta$-subunit complexes [31mer(−14Cys)BChl]$_2$ and [31mer(−6Cys)BChl]$_2$ with a $Q_y$ band at ∼820 nm and a weaker $Q_x$ band at ∼590 nm (Figure 4, black). The spectrum is essentially the same as that for the BChl-*a* dyad in either the native-sequence 31mer $\beta\beta$-subunit complex or the native $\alpha\beta$-subunit complex.[11,12] The key steps in forming the biohybrid complexes include (i) bioconjugation of chromophore X (**BC1**, **BC2**, **RR**, **OGR**) to 31mer(−14Cys) to form constructs 31mer(−14Cys)X, followed by (ii) interaction with BChl-*a* to assemble B820-type complexes [31mer(−14Cys)X/BChl]$_2$. The biohybrid complex [31mer(−6Cys)OGR/BChl]$_2$ was also assembled (see Experimental Procedures and Supporting Information).

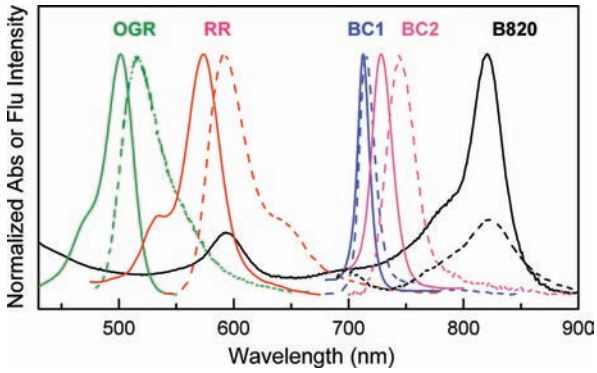


**Figure 4.** Normalized absorption (solid) and fluorescence (dashed) spectra of bioconjugatable dyes (colored) and of BChl-*a* dimer B820 in subunit complex [31mer(−14Cys)BChl]$_2$ (black). The B820 fluorescence is scaled arbitrarily for clarity.

Figure 5A shows part of the spectral evolution (black→green→red) obtained for the formation of biohybrid complex [31mer(−14Cys)OGR/BChl]$_2$. Comparison with Figure 4 shows that the complex combines the characteristic native-like B820 absorption and that of **OGR** at ∼500 nm. Figure 5A

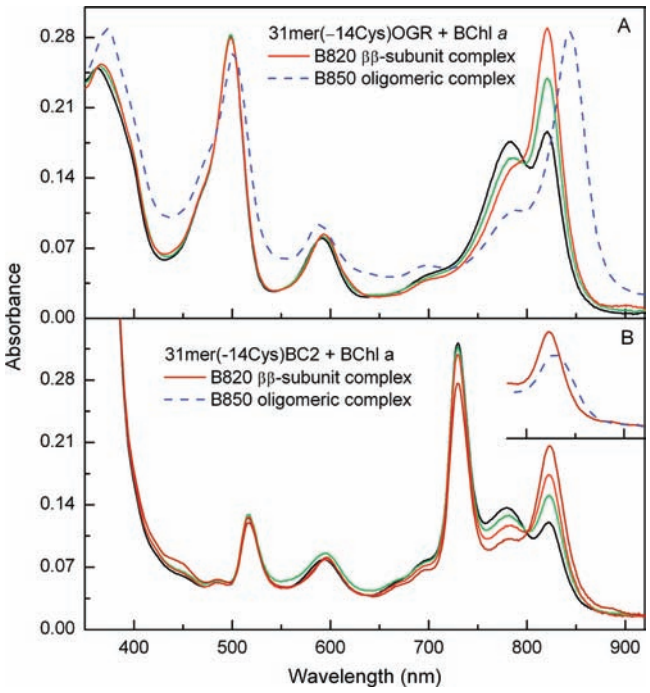


**Figure 5.** Absorption spectra for formation of B820- and B850-type complexes. (A) The solution contains 31mer(−14Cys)OGR and BChl-*a* at 0.90% (black), 0.75% (green), and 0.66% (red) octyl glucoside; the latter is then chilled overnight (dashed blue). (B) The solution contains 31mer(−14Cys)BC2 and BChl-*a* at 0.90% (black), 0.75% (green), and 0.66% (red) octyl glucoside; the latter is then chilled for 1 h (brown) or overnight (dashed blue).


dx.doi.org/10.1021/ja207390y | *J. Am. Chem. Soc.* 2012, 134, 4589−4599

also illustrates that chilling (typically overnight) results in association of $\beta\beta$-subunits to form an oligomeric complex [31mer-(−14Cys)OGR/BChl]$_n$ that has the $Q_y$ absorption shifted to ~850 nm; thus, the interacting BChl's of the oligomeric complex are generically denoted B850. The $\beta\beta$-subunit complex is re-formed by warming to room temperature. The oligomeric complex also can be stabilized at room temperature by first diluting the cold sample of the $\beta\beta$-subunit complex with cold buffer to decrease the detergent concentration to below its critical micelle concentration (CMC) and then warming the sample to room temperature. Formation of the analogous **BC2**-containing $\beta\beta$-subunit complex [31mer(−14Cys)BC2/BChl]$_2$ is shown in Figure 5B; **BC2** contributes the strong $Q_y$ band at 730 nm and modest $Q_x$ band at 515 nm. Similar behavior is found for constructs with **RR** and **BC1**, except that for the latter the oligomeric complex is stabilized at room temperature with the detergent concentration still slightly above the CMC.

The subunit and oligomeric complexes may contain extra absorption in the 780−800 nm and Soret regions (Figure 5) due in part to excess BChl-*a* sometimes used to saturate assembly formation. Additionally, the spectra of the $\beta\beta$-subunit complexes necessarily contain small amounts of free BChl-*a* and free peptide with bound pigment X [e.g., 31mer(−14Cys)X] because the formation/dissociation of the subunit complex is an equilibrium process. The equilibrium disassembly is substantially diminished upon formation of the oligomeric architectures.

**3.3. Energy-Transfer Characteristics of Dimeric Subunit (B820-Type) Complexes.** *3.3.1. Overview.* In this section, measurements are described on the B820-type $\beta\beta$-subunit complexes. The inherent properties of photoexcited B820 (B820*) in [31mer(−14Cys)BChl]$_2$ (no attached synthetic chromophore) are given first as a benchmark for results on the analogues [31mer(−14Cys)X/BChl]$_2$ that contain chromophore X (**OGR**, **RR**, **BC1**, or **BC2**). The homodimeric B820-type $\beta\beta$-subunit complexes can be sufficiently stabilized to be studied in detail, which has the following advantages. First and foremost, structural knowledge about the B820-type complex stems from extensive spectroscopic characterization[11,12,27−33] and crystal structures of two LH2 complexes[7,9] and that of an RC-LH1 core complex.[8] Any significant perturbation of the structure by a covalently added chromophore would be easily observable in the association constant[11,12] and spectroscopic properties of the B820 complex. While the flexible hydrocarbon tether permits some conformational freedom of the covalently attached chromophores, positions −14 and −6 were chosen for attachment because they are on a part of the polypeptide that must be $\alpha$-helical for appropriate BChl-*a* binding to form B820 (Figure 1). Second, the B820-type complex is in equilibrium with the "free" polypeptides and BChl-*a* so that thermodynamic measurements are possible.[11,12] Third, studies of the B820 complexes provide a benchmark for assembling and investigating oligomeric species (section 3.4).

*3.3.2. Control B820-Type Complexes.* Figure 6 shows time-resolved absorption data for [31mer(−14Cys)BChl]$_2$ obtained using a 0.1-ps excitation flash in the $Q_x$ band at 590 nm. The data reveal an instrument-limited rise and subsequent evolution in the combined feature associated with the bleaching in the B820 $Q_y$ absorption and B820* stimulated emission (fluorescence stimulated by the white light probe pulse). Figure 6A shows that B820* has completely decayed to the ground state ($\Delta A$ = 0) by 4 ns. Figure 6B and the short-time inset show kinetic traces representative of those acquired at 1.5-nm

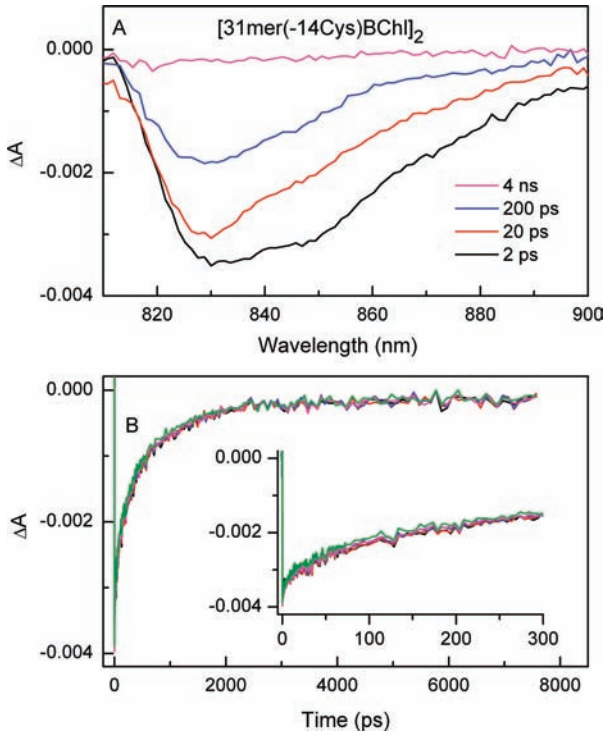


**Figure 6.** Time-resolved absorption spectra (A) and five kinetic traces between 829 and 834 nm (B) for [31mer(−14Cys)BChl]$_2$ ($\lambda_{exc}$ = 590 nm).

intervals from 800 to 900 nm. The data were globally analyzed using a triple-exponential function, resulting in best-fit time constants of 3, 50, and 600 ps.

The raw spectral data in Figure 6A, along with principal-component and global analysis, indicate that the 3-ps component has little decay of B820 $Q_y$ bleaching and thus little return of B820* to the ground state. Thus, this fast component likely reflects relaxation (vibrational, conformation, electronic) on the excited-state potential-energy surface, accompanied by a change in spectral shape (e.g., a shift in the stimulated emission position). The 50- and 600-ps components (relative amplitudes of 0.2 and 0.8 at 820 nm) both contribute to the time evolution across the 800−900-nm region and involve bleaching decay and thus deactivation of B820* to the ground state. One interpretation is that the major 600-ps component reflects the inherent decay of B820* and the minor 50-ps component reflects energy transfer followed by exciton annihilation (and ground-state recovery) involving two $\beta\beta$-subunit complexes in close contact. Such assignments would parallel those for decay components on these time scales for the excited BChl-*a* complex B850* in native LH2 complexes, with the shorter component reflecting LH2 clusters (which form depending on conditions such as detergent concentration).[34] Another interpretation, or a contribution to the B820* decay in [31mer(−14Cys)BChl]$_2$ on both time scales, is that there is more than one chromophore−peptide conformer with small differences in the spatial relationship of the two BChl-*a* that comprise B820, leading to multiple decay times.

The dominant 600-ps lifetime component of B820* decay in [31mer(−14Cys)BChl]$_2$, and the amplitude-weighted value of (0.2)(50 ps) + (0.8)(600 ps) ≈ 500 ps, are considerably shorter than the average (for many solvents) singlet excited-state lifetime of 3 ns for monomeric BChl-*a*.[35] Similarly, the B820


dx.doi.org/10.1021/ja207390y | J. Am. Chem. Soc. 2012, 134, 4589−4599

fluorescence yield of roughly 0.01 measured here for [31mer-(−14Cys)BChl]$_2$ is shorter than the average value of 0.17 for BChl-*a*.[35] The inherent decay (largely by internal conversion) of photoexcited BChl-*a* dimer (P870*) in the bacterial photosynthetic reaction center (measured when electron transfer is blocked) is also relatively short (100−200 ps) and heterogeneous in that the apparent lifetime varies about 2-fold with probe wavelength.[36] The shorter inherent B870* lifetime (in the absence of electron transfer) versus that for monomeric BChl-*a* has been ascribed to enhanced nuclear−electronic coupling (Born−Oppenheimer breakdown).[37] The rationale stems from the fact that the excited state of the tightly coupled BChl molecules ($B_a$ and $B_b$) is comprised of a linear combination of locally excited ($B_a$* and $B_b$*) and charge-transfer ($B_a^+ B_b^-$ and $B_a^- B_b^+$) configurations. The latter configurations are sensitive to motions that modulate the distance (and Coulombic interaction) between the two BChl-*a* molecules, resulting in vibration-induced fluctuations in the electronic character of B870* that enhance nonradiative deactivation. These same characteristics almost certainly apply to B820* in the biohybrid antenna complexes.

*3.3.3. OGR-Containing B820-Type Complexes.* Representative data for the **OGR**-containing complexes are shown in Figure 7. The right inset shows B820 fluorescence at ∼825 nm

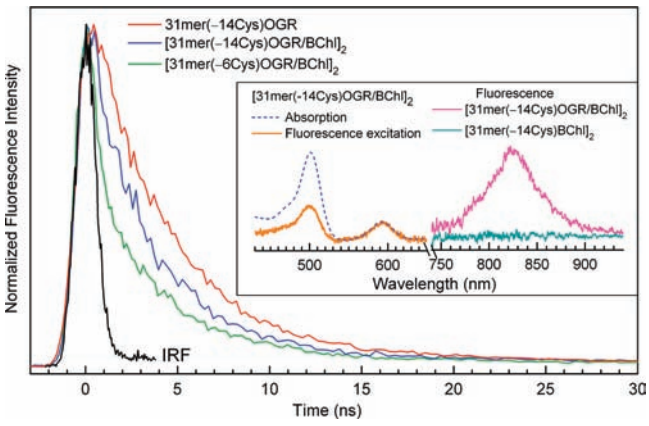


**Figure 7.** Photophysical data for OGR-containing controls and B820-type $\beta\beta$-subunit complexes. The main panel shows fluorescence decays ($\lambda_{exc}$ = 499 nm, $\lambda_{det}$ = 520 nm) for the control peptide (red) and biohybrids (blue, green) along with the instrument response function (IRF; black). The insets show fluorescence ($\lambda_{exc}$ = 494 nm), fluorescence excitation ($\lambda_{det}$ = 825 nm), and absorption spectra (see text).

elicited by excitation of **OGR** at 494 nm in biohybrid complex [31mer(−14Cys)OGR/BChl]$_2$ (magenta). That this emission is not due to direct excitation of B820 is demonstrated by its absence in the **OGR**-free control complex [31mer(−14Cys)-BChl]$_2$ (teal) studied under the same conditions ($\lambda_{exc}$, concentrations). The left inset of Figure 7 shows the excitation spectrum (430−650 nm) of the B820 fluorescence (orange) normalized to the absorption spectrum (dashed blue) in the B820 $Q_x$ band. The ratio of excitation to absorption signals (integrated intensities) at 500 nm for **OGR** gives $\Phi_{ENT}$ = 0.40.

Companion time-resolved fluorescence data are shown in the main part of Figure 7. The OGR* lifetime is reduced from 4.1 ns in 31mer(−14Cys)OGR control (red) to 3.2 ns in [31mer(−14Cys)OGR/BChl]$_2$ biohybrid (blue). The lifetime reduction gives $\Phi_{ENT}$ = 0.22. This result, together with that from steady-state emission, gives an average value of $\Phi_{ENT}$ = 0.3 for **OGR**→B820 energy transfer. Figure 7 also shows that more rapid energy transfer shortens the excited-state lifetime to ∼0.2 ns for **OGR** at the −6 position in [31mer(−6Cys)OGR/BChl]$_2$. A small ∼4-ns component is due to 31mer(−6Cys)-OGR formed by dissociation of the complex.

Although the OGR* decay profile for [31mer(−14Cys)-OGR/BChl]$_2$ in Figure 7 is well described by a single exponential with $\tau$ = 3.2 ns, a small 4.1-ns component due to free 31mer(−14Cys)OGR complex would not cause a detectable deviation from a single-exponential fit. For example, simulated data generated with a dual-exponential function—a small 4.1-ns component for free 31mer(−14Cys)OGR and a major 2.9-ns component for [31mer(−14Cys)OGR/BChl]$_2$—are fit well by a single exponential with $\tau$ = 3.2 ns (the same as observed). If the true lifetime for [31mer(−14Cys)OGR/BChl]$_2$ were 2.9 ns, the energy-transfer yield would then increase to 0.29 (from 0.22), which would be closer to the value of 0.40 obtained from fluorescence excitation spectra. Such considerations exemplify the good agreement of the two measurements of the energy-transfer efficiency within experimental uncertainty.

*3.3.4. BC2-Containing B820 Complexes.* Representative data for **BC2**-containing complexes are shown in Figures 8

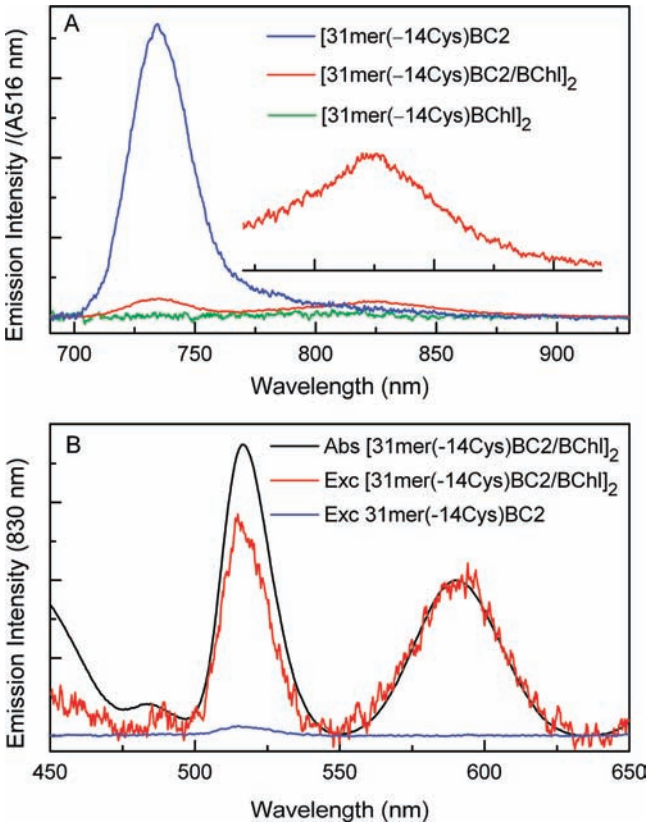


**Figure 8.** (A) Fluorescence spectra ($\lambda_{exc}$ = 516 nm) for peptide 31mer(−14Cys)BC2 (blue) and B820-type complexes [31mer(−14Cys)-BC2/BChl]$_2$ (red) and [31mer(−14Cys)BChl]$_2$ (green). The intensities are divided by the absorbance at $\lambda_{exc}$. The inset is a blowup of the NIR emission of [31mer(−14Cys)BC2/BChl]$_2$. (B) Fluorescence excitation spectrum ($\lambda_{det}$ = 830 nm) of [31mer(−14Cys)BC2/BChl]$_2$ (red) normalized to the absorption spectrum at 590 nm (black), and the excitation spectrum of peptide 31mer(−14Cys)BC2 (blue) scaled by the **BC2** fluorescence yield relative to that in [31mer(−14Cys)BC2/BChl]$_2$.

and 9. Figure 8A shows fluorescence spectra for [31mer-(−14Cys)BC2/BChl]$_2$ (red) and 31mer(−14Cys)BC2 (blue)


dx.doi.org/10.1021/ja207390y | J. Am. Chem. Soc. 2012, 134, 4589−4599

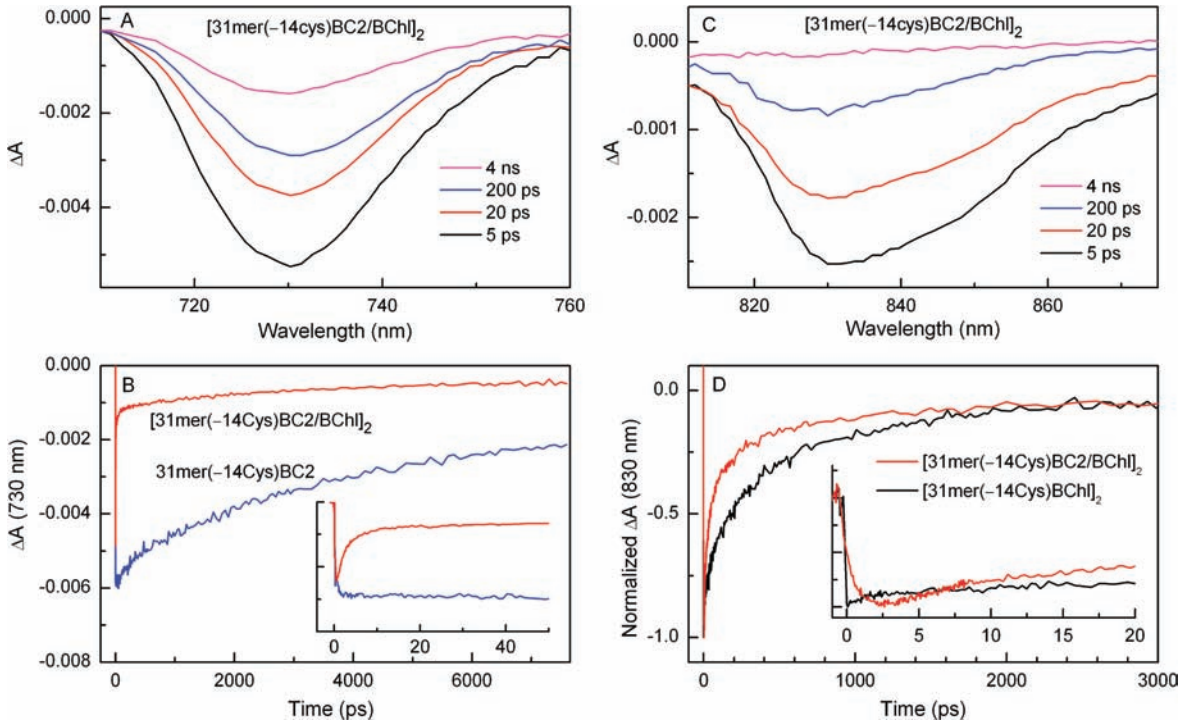


**Figure 9.** Time-resolved absorption spectra for $[31mer(-14Cys)BC2/BChl]_2$ in the $Q_y$ bleach and stimulated emission for **BC2** (A) and B820 (C) and corresponding kinetic traces at 730 nm (B) and 830 nm (D) for $[31mer(-14Cys)BC2/BChl]_2$ (red) and 31mer(−14Cys)BC2 (blue) using $\lambda_{exc}$ = 512 nm. The kinetic trace in D for $[31mer(-14Cys)BChl]_2$ (black) utilizes $\lambda_{exc}$ = 590 nm and $\lambda_{det}$ = 830 nm.

obtained using excitation in the $Q_x$ band of **BC2** at 516 nm. The feature at 740 nm is **BC2** fluorescence. As expected, no emission is observed from **BC2**-free $[31mer(-14Cys)BChl]_2$ (green). The fluorescence intensity of each sample was divided by the (similar) absorbance at $\lambda_{exc}$. The ratio of the integrated (690−770 nm) intensities reveals that the **BC2** fluorescence from $[31mer(-14Cys)BC2/BChl]_2$ is 8% of that from 31mer(−14Cys)BC2. This reduction corresponds to $\Phi_{ENT}$ = 0.92 for **BC2**→B820 energy transfer in the biohybrid.

Figure 8A (and inset) also shows that excitation of **BC2** at 516 nm gives rise to B820 fluorescence at ∼830 nm in $[31mer(-14Cys)BC2/BChl]_2$ but not in the controls, again reflecting energy transfer in the biohybrid. Figure 8B shows the fluorescence excitation spectrum ($\lambda_{det}$ = 830 nm) normalized to the absorption spectrum at 590 nm. Comparison of the integrated (490−550 nm) areas of the $Q_x$ band of **BC2** in the excitation versus absorption spectra gives $\Phi_{ENT}$ = 0.75 for **BC2**→B820 energy transfer. This value is modestly lower than that obtained from the **BC2** fluorescence quenching.

A third estimate for $\Phi_{ENT}$ is provided by transient absorption measurements of the BC2* lifetime in the absence and presence of energy transfer. Figure 9A shows representative spectra ($\lambda_{exc}$ = 512 nm) that contain combined **BC2** $Q_y$ bleaching and stimulated emission. Figure 9B and the short-time inset show time profiles at 730 nm for biohybrid $[31mer(-14Cys)BC2/BChl]_2$ (red) and control peptide 31mer(−14Cys)BC2 (blue). The BC2* decay profile for the control peptide is well described by a single exponential with $\tau$ = 4 ns, similar to that obtained from fluorescence decay for this same peptide as well as for **BC2** in buffer solution by both techniques. For $[31mer(-14Cys)BC2/BChl]_2$, about 15% of BC2* decay also has $\tau \approx 4$ ns, which can be attributed to free 31mer(−14Cys)BC2 formed by dissociation of the complex. Most of the BC2* decay occurs in <100 ps, with time constants (and relative fractions) of 3 ps (0.60) and 30 ps (0.25). The non-single-exponential BC2* decay in the biohybrid likely reflects more than one conformation of **BC2** with respect to B820 due to linker mobility. The rapid (<100 ps) decay compared to 4 ns in the control peptide indicates that **BC2**→B820 energy transfer in $[31mer(-14Cys)BC2/BChl]_2$ has $\Phi_{ENT}$ > 0.95. This estimate together with 0.92 from **BC2** fluorescence quenching and 0.75 from excitation-spectrum analysis give a collective $\Phi_{ENT}$ = 0.9.

Energy transfer from **BC2** to B820 produces B820* and associated B820 $Q_y$ bleaching and B820* stimulated emission (Figure 9C). The B820* time profile for $[31mer(-14Cys)BC2/BChl]_2$ (Figure 9D and inset, red) shows an ∼1 ps (non-instantaneous) rise followed by components of roughly 3, 30, and 600 ps. Although simple B820* rise and fall kinetics are not expected in the biohybrid because the BC2* decay in this system is multiexponential (3 and 30 ps) and the inherent time evolution of B820* (obtained in $[31mer(-14Cys)\ BChl]_2$) is multiexponential (3, 50, and 600 ps), the time profile contains recognizable characteristics. The B820* rise in $[31mer(-14Cys)BC2/BChl]_2$ (Figure 9D inset, red) occurs in ∼1 ps, which is a manifestation of **BC2**→B820 energy transfer, compared to the instantaneous (<150 fs) response obtained upon direct excitation ($\lambda_{exc}$ = 590 nm) of B820 in $[31mer(-14Cys)BChl]_2$ (Figure 9D, inset black). This rise and the subsequent ∼3 ps component reflect the convolution of the early time decay components of BC2* decay and the inherent B820* time evolution, and similarly for the overlapping components over tens of picoseconds. The decay component on the time scale of hundreds of picoseconds in the biohybrid is similar to the component of the inherent decay of B820*. The presence of this longer-time phase for $[31mer(-14Cys)BC2/BChl]_2$ suggests that B820* does not undergo significant (and


dx.doi.org/10.1021/ja207390y | J. Am. Chem. Soc. 2012, 134, 4589−4599

unwanted) quenching by **BC2** following **BC2**→B820 energy transfer.

*3.3.5. RR-Containing B820-Type Complexes.* Energy transfer from **RR** to B820 was probed in $\beta\beta$-subunit complex [31mer(−14Cys)RR/BChl]$_2$. The analysis for most measurements parallels that for the **OGR**- and **BC2**-containing analogues. For example, excitation of **RR** at 526 nm leads to B820 fluorescence at 830 nm (Figure S-3A). This process results in quenching of the **RR** fluorescence at 580 nm compared to control peptide 31mer(−14Cys)RR, affording $\Phi_{ENT}$ = 0.70. Comparison of the normalized and integrated B820 fluorescence excitation spectrum and the absorption spectrum across the **RR** profile centered at 580 nm gives $\Phi_{ENT}$ = 0.55 (Figure S-3B). Time-resolved absorption studies (Figures S-4 and S-5) show that the RR* decay in [31mer(−14Cys)RR/BChl]$_2$, control peptide 31mer(−14Cys)RR, and RR alone in solution all require fitting by three exponentials. The reduced amplitude-weighted lifetime for the biohybrid versus the control affords $\Phi_{ENT}$ = 0.60 (see Supporting Information). The three independent assays give consistent results and an average of $\Phi_{ENT}$ = 0.6.

**3.4. Energy-Transfer Characteristics of Oligomeric (B850-Type) Complexes.** *3.4.1. Overview.* The studies described above have focused on homodimeric B820-type complexes. We now turn to the study of oligomeric species, for which there are some advantageous properties exhibited by native systems. In the reconstitution of LH1 and LH2 with native polypeptides and BChl,[11,12] the bathochromically shifted $Q_y$ absorption and circular dichroism spectra reproduce the values observed *in vivo*, and therefore the reconstituted systems very likely have cyclic structures as observed in crystal structures and atomic-force microscopy of these complexes.[7−9] The native LH1 and LH2 complexes are oligomers of $\alpha\beta$-heterodimeric B820 subunits in which there are specific stabilizing interactions between the two polypeptides in their N-terminal regions.[38] The polypeptides studied here do not have the full N-terminal portion of the native *Rb. sphaeroides* LH1 $\beta$-polypeptide and thus would not form native oligomeric structures with a native $\alpha$-polypeptide.[11,12] However, the homodimeric $\beta\beta$-B820 species do associate when the detergent concentration is lowered below the CMC and form oligomeric species with bathochromically shifted $Q_y$ bands compared to the B820 subunit form.[23,24,39] The extent of this bathochromic shift has been related to the number of interacting BChl-*a* in the oligomeric species.[40] Whether the oligomers form rings of 8 or 9 subunits (16 or 18 BChl-*a*) like LH2 when the $Q_y$ maximum is near 850 nm, or whether smaller numbers of subunits are associated to form "arcs",[40] is not known at this time. The oligomeric forms of the $\beta\beta$-homodimers are usually very stable at low temperature (at 0.66% octyl glucoside) or at room temperature when the octyl glucoside concentration is lowered to below the CMC (e.g., 0.33%).

The biohybrids containing **OGR**, **RR**, and **BC1** form oligomers that have a substantially bathochromically shifted $Q_y$ band (847, 845, and 844 nm; see Figures 5A and S-9 for the **OGR** and **BC1** complexes), whereas for **BC2** the absorption maximum shifts to between 830 and 835 nm; see Figure 5B). The bathochromic shift in the $Q_y$ band simplifies photophysical studies compared to B820-type complexes due to (i) reduced overlap with the absorption and emission bands of free BChl-*a* (absorbing at 780 nm) and (ii) a greater shift from the 800-nm light used to generate the continuum probe pulses in ultrafast absorption studies. In the following, results are presented concerning the oligomeric assemblies, first those containing B850 without a bioconjugated chromophore and then with attached **OGR** or **RR**. These B850-type complexes are stabilized at room temperature (by dilution of the detergent rather than chilling alone) to facilitate comparisons with the results presented above on the B820-type analogues studied at the same temperature.

*3.4.2. The BChl-a Oligomer B850.* The time-resolved absorption data for the B850 $Q_y$ bleach and B850* stimulated emission decay in oligomer [31mer(−14Cys)BChl]$_n$ are given in Figure S-8. The characteristics are generally similar to those for B820 in the $\beta\beta$-subunit complex [31mer(−14Cys)BChl]$_2$ (Figure 6) except for a bathochromic shift in the spectral features and more rapid overall decay to the ground state. The time evolution for B850* (like B820*) requires fitting with (minimally) three exponentials, giving time constants of 6, 40, and 500 ps. The 6-ps component for B850*, like the 3-ps component for B820*, is attributed to relaxation (vibrational, conformational, electronic) on the excited-state potential-energy surface with little if any decay to the ground state. The 40- and 500-ps components (relative amplitudes of 0.7 and 0.3 at 850 nm) both contribute to the time evolution across the 800−900 nm region and involve bleaching decay and thus deactivation of B850* to the ground state. Heterogeneity in the decay kinetics of B850* is analogous to that discussed above for B820*.

The chief finding is that B850* in oligomer complex [31mer(−14Cys)BChl]$_n$ decays more rapidly than B820* in $\beta\beta$-subunit complex [31mer(−14Cys)BChl]$_2$. This observation is in keeping with the fluorescence yields of ∼0.001 for B850 and ∼0.01 for B820 determined here. Enhanced nonradiative deactivation driving diminished $\tau_S$* and $\Phi_f$ for B850* versus B820* (and versus 3 ns and 0.17 for monomeric BChl-*a*) could arise from (i) nuclear−electronic coupling as described above for B820* but now involving a greater number and perhaps more highly interacting BChl-*a* molecules, (ii) the energy-gap law for nonradiative decay[41] associated with the lower excited-state energy, and (iii) greater effective clustering of the complexes leading to increased exciton annihilation.

*3.4.3. OGR-Containing Oligomeric Complexes.* The results of photophysical measurements on [31mer(−14Cys)OGR/BChl]$_n$ are shown in Figure 10. The data can be compared directly with those described above for [31mer(−14Cys)OGR/BChl]$_2$ (Figure 7) and are analyzed similarly. The OGR* lifetime of 3.4 ns for [31mer(−14Cys)OGR/BChl]$_n$ versus 4.1 ns for 31mer(−14Cys)OGR gives $\Phi_{ENT}$ = 0.17. The normalized fluorescence excitation and absorption spectra gives $\Phi_{ENT}$ = 0.22. The average value is 0.2. The values of $\beta\beta$-subunit complex determined above for the B820-type complex are 0.22 (fluorescence lifetimes) and 0.40 (excitation/absorption spectra), for an average of 0.3. Thus, the efficiency of energy transfer from **OGR** to B850 in the oligomeric biohybrid is comparable to or slightly lower than that from **OGR** to B820 in the $\beta\beta$-subunit form.

*3.4.4. RR-Containing Oligomeric Complexes.* Photophysical studies were performed on **RR**-containing oligomeric complexes and controls (Figures S-6 and S-7) that are analogous to those described above for the **RR**-containing $\beta\beta$-subunit complexes (Figures S-3 and S-5). The reduction of **RR** fluorescence in [31mer(−14Cys)RR/BChl]$_n$ versus 31mer(−14Cys)RR gives $\Phi_{ENT}$ = 0.90. The normalized fluorescence excitation and absorption spectra give $\Phi_{ENT}$ = 0.58.

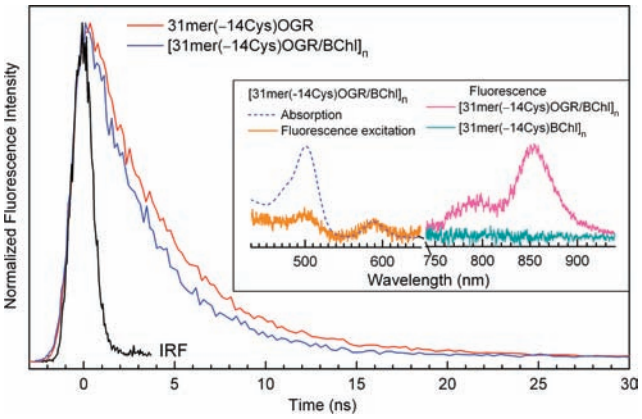


**Figure 10.** Photophysical data for **OGR**-containing controls and B850-type oligomeric complex. The main panel shows fluorescence decays ($\lambda_{exc}$ = 499 nm, $\lambda_{det}$ = 520 nm) for the control peptide (red) and the biohybrid (blue) along with the instrument response function (IRF; black). The insets show fluorescence, fluorescence excitation, and absorption data as indicated and described in the text.

Time-resolved absorption studies afford $\Phi_{ENT}$ = 0.93 (see Supporting Information for analysis). The three measurements afford an average value of $\Phi_{ENT} \approx 0.8$ for **RR**→B850 energy transfer in oligomeric assembly [31mer(−14Cys)RR/BChl]$_n$. This result can be compared with the average value of $\Phi_{ENT}$ = 0.6 for **RR**→B820 energy transfer in $\beta\beta$-subunit complex [31mer(−14Cys)RR/BChl]$_2$. Collectively, the results indicate that the efficiency of energy transfer is comparable to or somewhat greater in the oligomeric assembly than in the subunit complex.

*3.4.5. BC1-Containing Oligomeric Complexes.* Oligomeric complexes containing **BC1** are very stable at room temperature, even with the detergent concentration still slightly above the CMC, and heating (e.g., at 35 °C) is required for conversion to the subunit form (see Figure S-9 for absorption spectra). Thus, studies on these systems focused on oligomeric complexes [31mer(−14Cys)BC1/BChl]$_n$. Measurements similar to those described above were used to determine the yield of **BC1**→B850 energy transfer, which give values of 0.87 from the **BC1** fluorescence-intensity quenching (Figure S-10A), 0.79 from **BC1** fluorescence excitation versus absorption spectra (Figure S-10B), and 0.94 from BC1* decay kinetics in the oligomer versus the peptide control. The average value is $\Phi_{ENT}$ = 0.9. Following excitation of **BC1**, B850 bleaching and decay are observed (Figure S-11). Thus, oligomeric complexes containing the synthetic bacteriochlorins combine strong NIR absorption and a high energy-transfer efficiency to the BChl-*a* acceptor complex.

**3.5. Comparison of the Energy-Transfer Characteristics of the Various Biohybrids.** All of the $\beta\beta$-subunit complexes exhibit energy transfer from the synthetic chromophore to the native-like BChl-*a* dimer B820. The energy-transfer efficiencies ($\Phi_{ENT}$ ± 0.1) for biohybrids [31mer(−14Cys)X/BChl]$_2$ increase in the following order for tethered chromophore X: **OGR** (0.3) < **RR** (0.6) < **BC2** (0.9). Similarly, the energy-transfer efficiencies observed in the oligomeric assemblies [31mer(−14Cys)X/BChl]$_n$ investigated increase in the order **OGR** (0.2) < **RR** (0.8) < **BC1** (0.9). The latter results show that the energy-transfer efficiencies in the oligomeric architectures are comparable to those in the subunit complexes. Additionally, $\Phi_{ENT}$ increases from 0.3 for **OGR** at the −14 position in [31mer(−14Cys)OGR/BChl]$_2$ to 0.8 for **OGR** at the −6 position in [31mer(−6Cys)OGR/BChl]$_2$.

These trends in the measured $\Phi_{ENT}$ values are consistent with a Förster through-space mechanism for energy transfer. Calculated $\Phi_{ENT}$ values obtained using PhotochemCad[42] are given for a range of distances in Table 1. Inspection of the calculated values using a 40 Å donor−acceptor center-to-center

**Table 1. Förster Energy-Transfer Parameters for B820-Type Biohybrid Complexes**[a]

| biohybrid system | donor $\Phi_f$ | donor $\tau_S$ (ns) | $(k_{rad})^{-1}$ (ns) | $J$ ($\times 10^{-13}$ cm$^6$) | $R$ (Å) | $\Phi_{ENT}$ |
|---|---|---|---|---|---|---|
| [31mer(−14Cys)BC2/BChl]$_2$ | 0.19 | 4.2 | 22 | 13 | 50 | 0.83 |
| | | | | | 40 | 0.95 |
| | | | | | 30 | 0.99 |
| | | | | | 20 | >0.99 |
| [31mer(−14Cys)BC1/BChl]$_2$ | 0.10 | 4.7 | 47 | 9.4 | 50 | 0.65 |
| | | | | | 40 | 0.88 |
| | | | | | 30 | 0.98 |
| | | | | | 20 | 0.99 |
| [31mer(−14Cys)RR/BChl]$_2$ | 0.14 | 2.4 | 17 | 4.4 | 50 | 0.55 |
| | | | | | 40 | 0.82 |
| | | | | | 30 | 0.96 |
| | | | | | 20 | 0.99 |
| [31mer(−14Cys)OGR/BChl]$_2$ | 0.058 | 4.1 | 71 | 1.5 | 50 | 0.15 |
| | | | | | 40 | 0.40 |
| | | | | | 30 | 0.79 |
| | | | | | 20 | 0.98 |
| [31mer(−6Cys)OGR/BChl]$_2$ | 0.058 | 4.1 | 71 | 1.5 | 25 | 0.92 |

[a]The energy-transfer efficiency ($\Phi_{ENT}$) for each of the biohybrid $\beta\beta$-subunit complexes [31mer(−14Cys)X/BChl]$_2$ (X = **OGR**, **RR**, **BC1**, **BC2**) and [31mer(−6Cys)OGR/BChl]$_2$ was calculated using PhotochemCad.[42] The input parameters for the energy are the fluorescence quantum yield ($\Phi_f$) and emission spectrum of the control peptide 31mer(−14Cys)X that contain chromophores X. The input parameters for the energy acceptor include the absorption spectrum of the BChl-*a* dimer B820 in the synthetic chromophore-free complex [31mer(−14Cys)BChl]$_2$. The calculations did not make use of the donor singlet excited-state lifetime ($\tau_S$) in the absence of the acceptor, which was used only to calculate the radiative rate constant $k_{rad} = \Phi_f/\tau_S$ listed in the table. Because $k_{rad}$ reflects the optical transition dipole strength of the donor, it is a useful parameter in gauging the relative effectiveness of the four chromophores in the Förster through-space dipole−dipole mechanism. See the Supporting Information for further information.


dx.doi.org/10.1021/ja207390y | J. Am. Chem. Soc. 2012, 134, 4589−4599

distance for the sake of discussion shows that the trend in calculated $\Phi_{ENT}$ for the series of chromophores at the −14 position reproduces the trend in measured values on the basis of the following parameters: (i) spectral overlap ($J$) of the chromophore (donor) fluorescence with the B820 (acceptor) absorption, and (ii) the chromophore radiative rate constant $k_{rad} = \Phi_f\tau_S$, which is driven largely by the differences in $\Phi_f$. A greater $\Phi_{ENT}$ value for **OGR** at the −6 versus −14 position is expected due to the shorter distance from the B820 energy acceptor (e.g., 25 versus 40 Å).

The effective chromophore−B820 distance is uncertain due to factors that include the flexibility (and nature) of the linker. A distance of 35−40 Å would be consistent with a fully extended 10 Å linker and the chromophore centered at 270° from the peptide axis (with 0° pointing from the −14Cys to the 0His site). The calculations also assume a dynamically averaged orientation factor of 1.125, which may not be correct and could differ for the various chromophores (and linkers). Thus, the calculations are not meant to serve as a structural probe. Collectively, the consistency of the trends in measured and calculated values is good and provides additional foundation for engineering the chromophores and assemblies to provide efficient energy transfer and solar coverage.

## 4. CONCLUSIONS AND OUTLOOK

The finding of rapid and highly efficient energy transfer ($\Phi_{ENT} \approx$ 90%) from tethered bacteriochlorins **BC1** and **BC2** to the native-like BChl-*a* acceptor complex, and the good yields for accessory chromophores (**OGR** and **RR**), augurs well for the use of such constructs as a foundation for producing more elaborate biohybrid light-harvesting architectures. For example, the simple 31mer $\beta\beta$-subunits of the type studied here could be employed in liposomes for improved stability, or the full-length $\alpha$ and $\beta$ polypeptides could be engineered to incorporate synthetic chromophores. The co-recognition of the $\alpha$ and $\beta$ polypeptides to form $\alpha\beta$-subunits and assembly of the latter affords highly stable native-like cyclic oligomeric architectures in which the $Q_y$ band of the BChl-*a* acceptor complex is at ∼870 nm. This wavelength is bathochromically shifted even farther versus that of the $\beta\beta$-subunit complexes (∼820 nm) or the oligomers assembled from the 31mer $\beta$ polypeptide (∼850 nm). Such stable oligomeric complexes provide a platform for further manipulations to achieve long-range directed energy flow, including patterning on surfaces as has been achieved with native antenna.[43] For biohybrid designs, dozens of stable, synthetic hydroporphyrins (chlorins, bacteriochlorins, and analogues) that together have absorption and fluorescence bands spaced in fine increments spanning the orange-red into the NIR regions (610−820 nm) are now available[15−19] and can be adapted for bioconjugation, as exemplified for **BC1** and **BC2** in Figure 4. This palette of chromophores enables the construction of a variety of oligomeric multi-subunit biohybrid architectures with various subunits housing distinct (bacterio)-chlorins with complementary absorption spectra. Such constructs rely on the natural light-harvesting antenna protein for the architectural scaffold. While our chief focus has concerned use of bioconjugatable bacteriochlorins given their attractive spectral and photophysical features, a very broad range of pigments should be amenable to this biohybrid approach. In summary, the ability to retain the superb features of native photosynthetic antenna complexes and achieve wide tunability in solar coverage via incorporation of synthetic chromophores, including the recently available NIR-absorbing bacteriochlorins, together may open new horizons in artificial photosynthesis.

## ■ ASSOCIATED CONTENT

### Supporting Information

Additional experimental procedures; analysis of data for **RR**-containing constructs; parameters for Förster calculations; complete ref 1; and additional data. This material is available free of charge via the Internet at http://pubs.acs.org.

## ■ AUTHOR INFORMATION


### Corresponding Author

p-loach@northwestern.edu; holten@wustl.edu; jlindsey@ncsu.edu; david.bocian@ucr.edu


### Notes

The authors declare no competing financial interest.

## ■ ACKNOWLEDGMENTS

This research was carried out as part of the Photosynthetic Antenna Research Center (PARC), an Energy Frontier Research Center funded by the U.S. Department of Energy, Office of Science, Office of Basic Energy Sciences, under Award No. DE-SC0001035.

## ■ REFERENCES


(1) Blankenship, R. E.; et al. *Science* **2011**, *332*, 805−809.

(2) Gabrielsen, M.; Gardiner, A. T.; Cogdell, R. J. In *The Purple Phototrophic Bacteria*; Hunter, C. N., Daldal, F., Thurnauer, M. C., Beatty, J. T., Eds.; Advances in Photosynthesis and Respiration; Springer: Dordrecht, The Netherlands, 2009; pp 135−153.

(3) Bullough, P. A.; Qian, P.; Hunter, C. N. In *The Purple Phototrophic Bacteria*; Hunter, C. N.; Daldal, F., Thurnauer, M. C., Beatty, J. T., Eds.; Advances in Photosynthesis and Respiration; Springer: Dordrecht, The Netherlands, 2009; pp 155−179.

(4) (a) Harvey, P. D.; Stern, C.; Guilard, R. In *Handbook of Porphyrin Science*; Kadish, K. M., Smith, K. M., Guilard, R., Eds.; World Scientific Publishing Co.: Singapore, 2011; Vol. *11*, pp 1−179. (b) Aratani, N.; Osuka, A. In *Handbook of Porphyrin Science*; Kadish, K. M., Smith, K. M., Guilard, R., Eds.; World Scientific Publishing Co.: Singapore, 2010; Vol. *1*, pp 1−132. (c) Moore, T. A.; Moore, A. L.; Gust, D. *Philos. Trans. R. Soc. London B* **2002**, *357*, 1481−1498. (d) Wasielewski, M. R. In *Chlorophylls*; Scheer, H., Ed.; CRC Press: Boca Raton, FL, 1991; pp 269−286.

(5) (a) Noy, D.; Moser, C. C.; Dutton, P. L. In *Chlorophylls and Bacteriochlorophylls: Biochemistry, Biophysics, Functions and Applications*; Grimm, B., Porra, R. J., Rüdiger, W., Scheer, H., Eds.; Springer: Dordrecht, The Netherlands, 2006; pp 349−363. (b) Nango, M. In *Chlorophylls and Bacteriochlorophylls: Biochemistry, Biophysics, Functions and Applications*; Grimm, B., Porra, R. J., Rüdiger, W., Scheer, H., Eds.; Springer: Dordrecht, The Netherlands, 2006; pp 365−373.

(6) Lindsey, J. S.; Mass, O.; Chen, C.-Y. *New J. Chem.* **2011**, *35*, 511−516.

(7) Papiz, M. Z.; Prince, S. M.; Howard, T.; Cogdell, R. J.; Isaacs, N. W. *J. Mol. Biol.* **2003**, *326*, 1523−1538.

(8) Roszak, A. W.; Howard, T. D.; Southall, J.; Gardiner, A. T.; Law, C. J.; Isaacs, N. W.; Cogdell, R. J. *Science* **2003**, *302*, 1969−1972.

(9) Koepke, J.; Hu, X.; Muenke, C.; Schulten, K.; Michel, H. *Structure* **1996**, *4*, 581−597.

(10) (a) Sturgis, J. N.; Tucker, J. D.; Olsen, J. D.; Hunter, C. N.; Niederman, R. A. *Biochemistry* **2009**, *48*, 3679−3698. (b) Sener, M. K.; Olsen, J. D.; Hunter, C. N.; Schulten, K. *Proc. Natl. Acad. Sci. U.S.A.* **2007**, *104*, 15723−15728.

(11) Loach, P. A.; Parkes-Loach, P. S. In *Anoxygenic Photosynthetic Bacteria*; Blankenship, R. E., Madigan, M. T., Bauer, C. E., Eds.; Kluwer Academic Publishers: Boston, MA, 1995; pp 437−471.

(12) Loach, P. A.; Parkes-Loach, P. S. In *The Purple Phototrophic Bacteria*; Hunter, C. N., Daldal, F., Thurnauer, M. C., Beatty, J. T., Eds.; Advances in Photosynthesis and Respiration; Springer: Dordrecht, The Netherlands, 2009; pp 181−198.
(13) Law, C. J.; Chen, J.; Parkes-Loach, P. S.; Loach, P. A. *Photosynth. Res.* **2003**, *75*, 193−210.
(14) Paulsen, H. In *Chlorophylls and Bacteriochlorophylls: Biochemistry, Biophysics, Functions and Applications*; Grimm, B., Porra, R. J., Rüdiger, W., Scheer, H., Eds.; Springer: Dordrecht, The Netherlands, 2006; pp 375−385.
(15) Yang, E.; Kirmaier, C.; Krayer, M.; Taniguchi, M.; Kim, H.-J.; Diers, J. R.; Bocian, D. F.; Lindsey, J. S.; Holten, D. *J. Phys. Chem. B* **2011**, *115*, 10801−10816.
(16) Krayer, M.; Yang, E.; Diers, J. R.; Bocian, D. F.; Holten, D.; Lindsey, J. S. *New J. Chem.* **2011**, *35*, 587−601.
(17) Taniguchi, M.; Cramer, D. L.; Bhise, A. D.; Kee, H. L.; Bocian, D. F.; Holten, D.; Lindsey, J. S. *New J. Chem.* **2008**, *32*, 947−958.
(18) Kee, H. L.; Kirmaier, C.; Tang, Q.; Diers, J. R.; Muthiah, C.; Taniguchi, M.; Laha, J. K.; Ptaszek, M.; Lindsey, J. S.; Bocian, D. F.; Holten, D. *Photochem. Photobiol.* **2007**, *83*, 1125−1143.
(19) Kim, H.-J.; Lindsey, J. S. *J. Org. Chem.* **2005**, *70*, 5475−5486.
(20) Wagner, R. W.; Lindsey, J. S. *Pure Appl. Chem.* **1996**, *68*, 1373−1380.
(21) Sutton, J. M.; Clarke, O. J.; Fernandez, N.; Boyle, R. W. *Bioconjugate Chem.* **2002**, *13*, 249−263.
(22) Mironov, A. F.; Grin, M. A. *J. Porphyrins Phthalocyanines* **2008**, *12*, 1163−1172.
(23) Meadows, K. A.; Parkes-Loach, P. S.; Kehoe, J. W.; Loach, P. A. *Biochemistry* **1998**, *37*, 3411−3417.
(24) Meadows, K. A.; Iida, K.; Tsuda, K.; Recchia, P. A.; Heller, B. A.; Antonio, B.; Nango, M.; Loach, P. A. *Biochemistry* **1995**, *34*, 1559−1574.
(25) Parkes-Loach, P. S.; Sprinkle, J. R.; Loach, P. A. *Biochemistry* **1988**, *27*, 2718−2727.
(26) Wang, Z.-Y.; Gokan, K.; Kobayashi, M.; Nozawa, T. *J. Mol. Biol.* **2005**, *347*, 465−477.
(27) Sorgen, P. L.; Cahill, S. M.; Krueger-Koplin, R. D.; Krueger-Koplin, S. T.; Schenck, C. C.; Girvin, M. E. *Biochemistry* **2002**, *41*, 31−41.
(28) Conroy, M. J.; Westerhuis, W. H. J.; Parkes-Loach, P. S.; Loach, P. A.; Hunter, C. N.; Williamson, M. P. *J. Mol. Biol.* **2000**, *298*, 83−94.
(29) Robert, B. In *The Purple Phototrophic Bacteria*; Hunter, C. N., Daldal, F., Thurnauer, M. C., Beatty, J. T., Eds.; Advances in Photosynthesis and Respiration; Springer: Dordrecht, The Netherlands, 2009; pp 199−212.
(30) Sturgis, J. N.; Olsen, J. D.; Robert, B.; Hunter, C. N. *Biochemistry* **1997**, *36*, 2772−2778.
(31) van Mourik, F.; van der Oord, C. J. R.; Visscher, K. J.; Parkes-Loach, P. S.; Loach, P. A.; Visschers, R. W.; van Grondelle, R. *Biochim. Biophys. Acta* **1991**, *1059*, 111−119.
(32) Visschers, R. W.; Chang, M. C.; van Mourik, F.; Parkes-Loach, P. S.; Heller, B. A.; Loach, P. A.; van Grondelle, R. *Biochemistry* **1991**, *30*, 5734−5742.
(33) Chang, M. C.; Callahan, P. M.; Parkes-Loach, P. S.; Cotton, T. M.; Loach, P. A. *Biochemistry* **1990**, *29*, 421−429.
(34) (a) Pflock, T.; Dezi, M.; Venturoli, G.; Cogdell, R. J.; Köhler, J.; Oellerich, S. *Photosynth. Res.* **2008**, *95*, 291−298. (b) Shubert, A.; Stenstam, A.; Beenken, W. J. D.; Herek, J. L.; Cogdell, R. J.; Pullerits, T.; Sundström, V. *Biophys. J.* **2004**, *86*, 2363−2373. (c) Hunter, C. N.; Bergström, H.; van Grondelle, R.; Sundström, V. *Biochemistry* **1990**, *29*, 3203−3207.
(35) (a) Niedzwiedzki, D. M.; Blankenship, R. E. *Photosynth. Res.* **2010**, *106*, 227−238. (b) Musewald, C.; Hartwich, G.; Pöllinger-Dammer, F.; Lossau, H.; Scheer, H.; Michel-Beyerle, M. E. *J. Phys. Chem. B* **1998**, *102*, 8336−8342. (c) Becker, M.; Nagarajan, V.; Parson, W. W. *J. Am. Chem. Soc.* **1991**, *113*, 6840−6848. (d) Losev, A. P.; Sagun, E. I.; Kochubeev, G. A.; Nichiporovich, I. N. *J. Appl. Spectrosc.* **1986**, *45*, 798−803. (e) Connolly, J. S.; Samuel, E. B.; Janzen, A. F. *Photochem. Photobiol.* **1982**, *36*, 565−574.
(36) Chuang, J. I.; Boxer, S. G.; Holten, D.; Kirmaier, C. *J. Phys. Chem. B* **2008**, *112*, 5487−5499.
(37) McDowell, L. M.; Kirmaier, C.; Holten, D. *Biochim. Biophys. Acta* **1990**, *1020*, 239−246.
(38) Parkes-Loach, P. S.; Majeed, A. P.; Law, C. J.; Loach, P. A. *Biochemistry* **2004**, *43*, 7003−7016.
(39) Kehoe, J. W.; Meadows, K. A.; Parkes-Loach, P. S.; Loach, P. A. *Biochemistry* **1998**, *37*, 3418−3428.
(40) Westerhuis, W. H. J.; Sturgis, J. N.; Ratcliffe, E. C.; Hunter, C. N.; Niederman, R. A. *Biochemistry* **2002**, *41*, 8698−8707.
(41) Birks, J. B. *Photophysics of Aromatic Molecules*; Wiley-Interscience: London, 1970; pp 142−192.
(42) Dixon, J. M.; Taniguchi, M.; Lindsey, J. S. *Photochem. Photobiol.* **2005**, *81*, 212−213.
(43) (a) Iida, K.; Dewa, T.; Nango, M. In *The Purple Phototrophic Bacteria*; Hunter, C. N., Daldal, F., Thurnauer, M. C., Beatty, J. T., Eds.; Advances in Photosynthesis and Respiration; Springer: Dordrecht, The Netherlands, 2009; pp 861−875. (b) Escalante, M.; Zhao, Y.; Ludden, M. J. W.; Vermeij, R.; Olsen, J. D.; Berenschot, E.; Hunter, C. N.; Huskens, J.; Subramaniam, V.; Otto, C. *J. Am. Chem. Soc.* **2008**, *130*, 8892−8893.